Pázmány Péter Catholic University

Faculty of Information Technology and Bionics

Roska Tamás Doctoral School of Sciences and Technology

Balázs Széky

Analysis of Stromal Stem Cells in Healthy and Diseased Skin

Theses of the PhD Dissertation

Scientific Advisor: Dr. Krisztián Németh PhD

Scientific Co-advisor: Dr. Miklós Gyöngy PhD

Budapest

2024

1. Introduction

The human dermis provides the high regenerative potential of skin by maintaining several stem cell micro-niches [1]-[3]. Despite the remarkable cellular heterogeneity of the dermis, all layers of the dermis (papillary, reticular, subcutaneous) contain fibroblasts, which play central roles in the maintenance of the dermal connective tissue, adipocyte pool, wound healing, hair follicle- and epidermal cell homeostasis [4]. Among the heterogeneous pool of fibroblast, stromal fibroblast subsets with stem-cell characteristics were identified, such as dermal mesenchymal stem cells [5] and multilineage differentiation, stress enduring (MUSE) cells [6]. These stem cell subsets have remarkable multilineage differentiation potential and employ several molecular mechanisms for the modulation of inflammatory immune responses [7], [8]. On the other hand, little is known about the functions of these cells in the stromal compartments of skin cancers, especially malignant metastatic melanomas.

Fibroblasts emerging within the tumor microenvironment affect cancer growth and spreading by several ways, including the suppression of anti-tumor immune responses [9], [10], and promoting cancer progression via cytokines [11], chemokines [12], exosomes [13], extracellular matrix molecules [14] and growth factors [15]. These stromal cells residing in solid tumor niches are termed “cancer-associated fibroblasts” (CAFs) due to their intricate interactions with cancer cells. CAFs are generated in the tumor niche from multiple cellular sources, such as pericytes, local stromal cells, epithelial cells, and adipocytes [16]. Comprehensive phenotypic and functional analysis were reported of CAFs from breast cancer [17], gastrointestinal cancers [18], prostate cancers [19] and leukemias [20]. On the other hand, little is known on the molecular phenotype and functions of CAFs in aggressive, metastatic melanomas.

Malignant melanoma is an aggressive, therapy-resistant skin cancer with poor survival and prognosis [21]-[23]. Although the primary tumors can be effectively eradicated by surgical dissection, they develop into metastatic stage rapidly, within a short period of time, (usually 2-6 months). The tumor microenvironment of melanomas comprises several cell types, such as tumor-infiltrating macrophages, immunosuppressive T-cells, endothelial cells, cancer stem cells, and melanoma-associated fibroblasts [24]. Despite the emerging importance of MAFs in the promotion of melanoma growth, the molecular

markers, and cellular phenotypes of fibroblasts in malignant metastatic melanomas has not been comprehensively characterized yet. Furthermore, less information is available on the presence of stromal stem cells, their differentiation potential, as well as their contribution to the stromal supply and growth of melanomas.

Here, I've set out to analyze specific cellular markers –including canonical MSC markers and stromal stem cell markers- and tri-lineage differentiation potential of MAFs from subcutaneous melanoma metastases As the importance of SSEA3+ multilineage differentiating, stress enduring cells in tissue repair [25], local immuno-modulation [26] and melanocyte differentiation [27] has gained more attention in the past few years, I've extended my *in vitro* characterization experiments to the SSEA3+ subset, it's pluripotency and *in vitro* melanocyte lineage differentiation.

2. Specific Aims

Malignant metastatic melanomas are the deadliest skin cancers due to high drug resistance and fast spreading of tumor cells. Melanoma cells have strikingly high differentiation plasticity, which endows them with the ability to generate genetically heterogeneous cancer stem cell populations in the tumor microenvironment. Conversely, cancer associated fibroblasts have stable genotype, which makes them attractive targets for anti-cancer therapies. Although, limited information is available on the specific cellular markers enabling the identification and targeting of MAFs. Furthermore, little is known on the differentiation plasticity of MAFs and its implications on melanoma growth and spreading.

The purpose of my doctoral research was to analyze and compare the molecular phenotype and the stem cell characteristics of MAFs. Given that cell surface markers and lineage differentiation potential of MAFs are incompletely characterized, here I set out to address the following questions.

1. Which mesenchymal stromal/stem cell surface markers do MAFs have?
2. What is the difference between the tri-lineage differentiation potential of stromal stem cells in melanoma compared to normal skin?

Although, the SSEA3+ fibroblasts were identified in stromal niches, the presence, ratio, and pluripotency of those cells in melanoma has not been characterized yet. Furthermore, the generation of melanoma-competent melanocytic cells from SSEA3+ was not evaluated yet. Hence, I've sought to address, whether

3. Pluripotent MUSE cells are present among MAFs, and
4. If MUSE cells from melanoma undergo melanocyte lineage differentiation?

3. Experimental Procedures

Ethics Statement

Surgically removed tumors and naevi were obtained from patients at the Department of Dermatology, Venereology and Dermato-oncology, (Semmelweis University, Budapest, Hungary). Tissue samples were collected for research after obtaining the patient's informed consent. The study was conducted according to the Declaration of Helsinki principles and approved by the Hungarian Scientific and Research Ethics Committee of the Medical Research Council (ETT TUKEB; Decree No. 32/2007, supplements 32-2/2007 and 32-3/2007).

Fibroblast isolation from healthy skin and melanoma

Dermal fibroblasts (DFs) were isolated from non-tumorous skin tissue slices. Skin tissues pieces were exposed for 2 hours in dispase (Gibco, Gaithersburg, MT) at 37 °C. Then, the digested epidermis was removed by tweezers, and dermal tissue was digested in collagenase-dispase solution for 2 hours with vortexing every 15 minutes. The solution containing the digested tissue was filtered through a 70 μm strainer (provided by Greiner Bio-one Ltd, Mosonmagyaróvár, Hungary) to remove tissue aggregates. The obtained cell suspension was centrifuged (500 rpm, 5 minutes), and resuspended in DMEM containing 20% fetal bovine serum (FBS; Corning, Tewksbury, MA), 1% GlutaMax and 1% Pen/Strep (Gibco), followed by the seeding of the cells into tissue culture flasks. Cells were grown at 37 °C and 5% CO_2 and we changed half of the culture medium with fresh medium every third day.

MAFs were isolated from surgically removed melanomas after obtaining the patients informed consent. Tumorous tissue was dissected from dermis, epidermis, and subcutaneous fat, chopped into smaller pieces by scalpels, then digested in collagenase-dispase solution for 2 hours to obtain single cells. Tissue slices were vortexed every 15 minutes during the incubation in collagenase-dispase solution (Gibco). To remove large cell aggregates, the solution with the digested tissue was filtered through a 70 μm cell strainer and centrifuged at 400 rpm for 5 minutes. Cellular pellet was resuspended in low glucose Dulbecco's modified eagle medium (DMEM, by Sigma Aldrich, St. Louis, MO)

containing 10% fetal bovine serum and incubated in a 25 cm^2 tissue culture flask (Corning, New York, USA) at 37 °C for 30 minutes to promote the attachment of fibroblast cells on the bottom of the flask, and the enrichment of cancer cells in the supernatant. Then, supernatant containing floating cells was removed by serological pipette and deposited into a new 25 cm^2 cell culture flask. Adhered cells were supplied with DMEM (Sigma Aldrich) containing 20% FBS, 1% Pen/Strep and 1% GlutaMax (Gibco) before putting back into the cell incubator (37 °C, 5% CO_2). We changed half of the cell culture medium on MAF cells every third day.

Methods for *in vitro* characterization

Immunocytochemistry

For immunocytochemical staining, we fixed cells in 4% PFA for 15 minutes, followed by permeabilization with 0.2% Trinton X-100 (Sigma) for 15 minutes and blocking in 2% bovine serum albumin (BSA, Corning) for 1 hour. Cells were incubated overnight with the primary antibodies at 4 °C. For secondary staining we used goat anti-mouse Cy3 conjugated antibody (purchased from Sigma), or donkey anti-rabbit Cy3 conjugated secondary antibody (purchased from Sigma). Nuclei were stained with the DNA-binding dye 4',6-diamidino-2-phenyl-indole (DAPI).

For setting up antibody staining for ectodermal, mesodermal and endodermal markers, we used immortalized cells or cancer cell lines originating from the given lineage. We choose cell lines with robust lineage marker expression, minimal cell culture requirements and fast growth kinetics. For the staining ectodermal neural markers MAP2, ENO2 and Nestin, we used A172 glioblastoma cell lines, while ectodermal melanocytic marker melan-A was assayed on SKMEL-28 and MALME-3M melanoma cell lines. We used HEP3B hepatocellular carcinoma cells to optimize the immunostaining of endodermal markers alpha-fetoprotein (AFP) and albumin. NTERA2 teratocarcinoma cells were used as positive control to assay pluripotency markers (OCT3/4, NANOG, TRA-1-60) expression.

Quantitative Real-time Polymerase Chain Reaction (RT-qPCR) with TaqMan Probes:

RNA extraction from 500.000-2000.000 cells was performed by using RNeasy mini kit of Qiagen, (Hilden, Germany). Briefly, cellular samples were lysed with RLT-buffer, and nucleic acids were precipitated by ethanol. Genomic DNA was eliminated by treating the samples with DNAse1 at room temperature for 30 minutes, followed by washing the samples through RNA-binding spin columns with washing buffers RW and RPE. RNA samples were eluted from the spin columns by adding nuclease-free dH_2O. For cDNA-synthesis we reverse-transcribed 1 µg RNA by using the MMLV reverse-transcriptase enzyme provided by Promega with oligo-dT primers, (Madison, USA). We measured qPCR in Lightcycler® 480. The FAM-MGB conjugated TaqMan Probes (by Thermo Fisher Scientific) used are listed in Table 3.3. below. We used GAPDH as a house-keeping control. Reaction mixes were incubated at 50 °C for 2 minutes, followed by denaturation (95 °C, 10 minutes). For the amplification we used 40 cycles starting with 95 °C, 15 seconds, followed by 60 °C for, 1 minutes and 72 °C, 1 second. Undifferentiated cells were used as internal, (normalization) controls for the calculation of C_T values.

Flow Cytometry and Fluorescence-activated Cell Sorting (FACS)

For flow-cytometric analysis, 200.000 MAFs in flow cytometry tubes (Corning) were washed in phosphate-buffered saline (PBS), then the samples were centrifuged at 1000 rpm for 5 minutes and resuspended in flow cytometry buffer (PBS containing 2% FBS). MAFs were incubated with FC-receptor blocker (produced by Thermo Fischer) for 10 minutes, followed by incubation with primary antibodies for FITC-conjugated CD90, APC-conjugated CD271, PE-conjugated SSEA3 (all from eBioScience, California, USA) and viability dye 7-amino-actinomycin-D (7AAD Thermo Fisher) for 30 minutes. After incubation of MAFs with antibodies, cells were washed with flow-cytometry buffer and resuspended in 500 µl flow cytometry buffer before the measurements. Single colored samples stained for CD90-PE (eBioScience), CD105-APC, CD90-FITC, and cells treated with 100 % methanol followed by incubation with 7AAD were used as compensation controls, while unstained cells were used to set signal thresholds for positive cell populations.

For sorting SSEA3+ cells, we used biotinylated antibody against SSEA3 with PE-conjugated streptavidin, which binds biotin with high affinity, (Fig.1). 5-10 million MAF cells were used for FACS in single-cell suspension. Cells were washed in PBS and stained with fixable NIR viability dye (provided by Thermo Fischer) according to the manufacturer's instructions. Then, cells were washed in FACS buffer (0.5% BSA, 2mM EDTA, all from Sigma), and incubated with FC-receptor blocker (TruStain FcX Fc receptor blocker by BD Pharmingen, (San Diego, USA) for 10 minutes. FC-receptor blocking was followed by incubation with 10 ng/µl biotin-conjugated rat SSEA3 antibody (Thermo Fischer Scientific, Waltham, Massachusetts, MA) and 4 ng/µl FITC-conjugated mouse CD90 antibody (eBioScience) for 30 minutes at 4 °C. Cells were washed with FACS buffer, and 750 ng/ml PE-streptavidin (eBioScience) was added for 30 minutes. Excess dye was removed by washing in FACS buffer, and cells were resuspended in 0.5 mL FACS buffer before the measurement. For FACS we used MA900 FACS-sorter of Sony Biotechnology (San Diego, USA). Live (nIR-negative) cells were gated out from the main population appearing on the forward scatter/ side-scatter (FSC/SSC) plot, followed by setting a gate on CD90+SSEA3+ double stained cells.

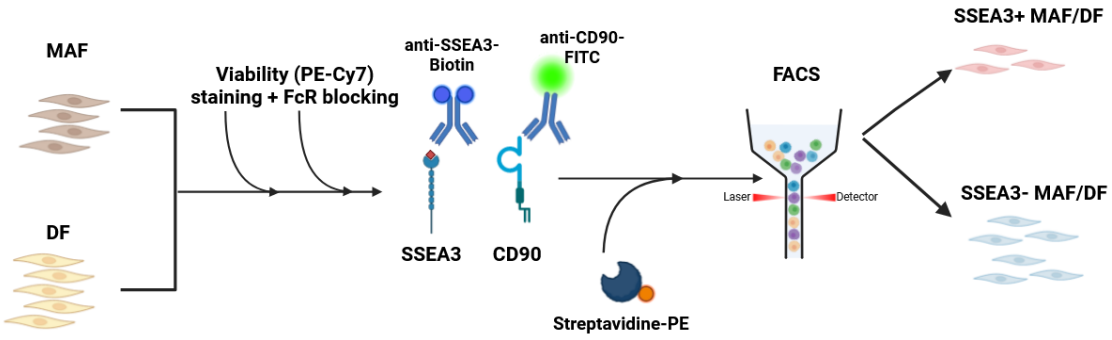

Figure 1. Labeling strategy for sorting SSEA3+CD90+ cells using FACS. *MAFs and DFs were stained for viability dye PE-Cy7, which was followed by FcR-blocking to avoid non-specific antibody binding to the Fc-receptors. After blocking, cells were incubated with biotin-conjugated anti-SSEA3 antibody and FITC-conjugated CD90+ antibody. To amplify the SSEA3 labeling, cells were incubated with PE-conjugated streptavidin. Both SSEA3+ and SSEA- cells were used for further experiments.*

In Vitro Differentiation Assays:

Ectodermal Lineage Differentiation

In Vitro Neural Lineage Differentiation:

To induce neural differentiation, 10^5 cells/cm^2 were seeded on ultra-low attachment plates (Corning) in completed neurobasal medium comprising of Neurobasal medium with 1 X B27 supplement, 1XN2 supplement, 1% Pen/Strep (all from Gibco) with 30 ng/mL epidermal growth factor and 30 ng/mL basic fibroblast growth factor (bFGF) (all from Peprotech, London, UK) added, (Fig.2). Medium was changed every other day. After 14 days of cultivation, spheres were collected and plated into poly-D-lysine-coated dishes for 10 days of neural induction in α-MEM supplemented with 2% FBS, 1% Pen/Strep, 25 ng/ mL bFGF and 25 ng/mL brain-derived neurotrophic factor (BDNF) (Peprotech). At the end of neural induction samples were processed for immunocytochemistry (ICC) and quantitative real-time polymerase chain reaction (qRT-PCR). A172 glioblastoma cells were used as positive control for ICC experiments. Mean intensities of ICC stainings for Nestin in undifferentiated MAFs, differentiated MAFs and A172 cells were quantified using ImageJ and normalized to the mean intensities of DAPI staining.

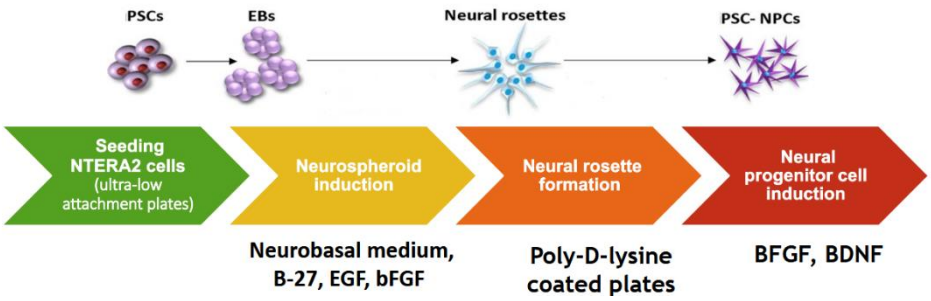

Figure 2. Overview of the differentiation protocol we devised for neural lineage differentiation of stem cells. *Pluripotent NTERA2 cells were used to optimize the in vitro neural differentiation assay. Embryoid bodies were generated from the cells on ultra-low attachment plates within 14 days in Neurobasal medium supplemented with B-27, N2, epidermal growth factor (EGF) and basic fibroblast growth factor (bFGF, FGF2). At day 14, spheres were transferred onto poly-D-lysine coated plates. Neural differentiation was induced by bFGF and BDNF in α-MEM medium containing 2% FBS.*

In vitro **Melanocyte Differentiation:**

For melanocytic differentiation, we used the protocol by Yamauchi et al, (2013) [28], (Fig.3). Sorted SSEA3+ and SSEA3- cells were seeded into fibronectin-coated dishes in DMEM containing 20% FBS, 1% GlutaMax and 1% Pen/Strep. On the next day, medium was switched to melanocytes differentiation medium, which is 50% high-glucose DMEM, 30% low glucose DMEM, 20% MCDB201 medium containing 0.05 M dexamethasone (Sigma-Aldrich, St Louis, MO), 100 µM L-ascorbic acid, 1 mg/ml linoleic acid–BSA, 1 ×insulin–transferrin–selenium (Invitrogen), 50 ng/ml SCF (R&D Systems, Minneapolis, MN), 10 ng/mL endothelin-3 (ET-3, Sigma-Aldrich), 50 ng/mL Wnt3a, 20 pM cholera toxin (Wako, Osaka, Japan), 50 nM 12-O-tetradecanoyl-phorbol 13-acetate (Sigma-Aldrich), and 4 ng/ml bFGF. Cells were differentiated in this melanocyte medium for 42 days. At day 42 of differentiation, cellular samples were processed for ICC and qRT-PCR.

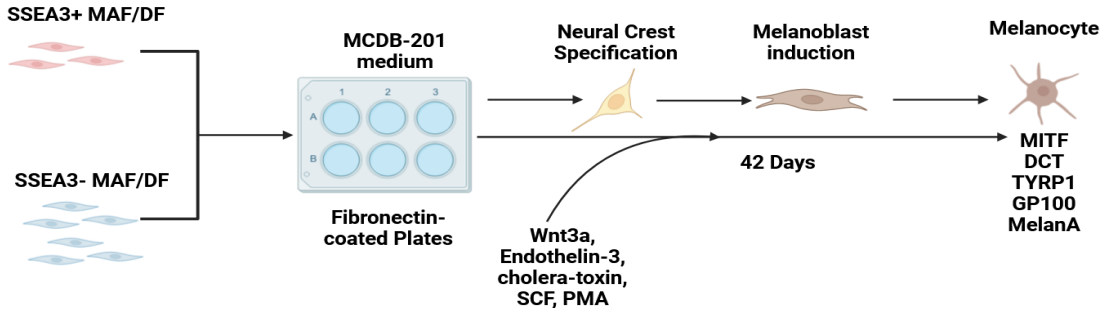

Figure 3. Method for in vitro melanocyte differentiation from SSEA3+ and SSEA3- cells, which were sorted from MAFs or DFs. *Cells were plated into fibronectin-coated plates and melanocytes differentiation was initiated by the addition of Wnt3a, Endothelin-3, SCF, PMA and cholera-toxin to the cell culture medium. Medium was changed every other day until day 42 of differentiation. On day 42, cells were characterized for the expression of melanocyte-specific markers.*

Mesodermal Lineage Differentiation

To induce osteogenic differentiation, 1000.000 MAFs were seeded into tissue-culture treated 6-well plates with DMEM supplemented with 10 nM dexamethasone, 100 µM ascorbic acid, 2 mM β-glycerophosphate (all from Sigma), 20% FBS, 1% P/S and 1% GlutaMax (Gibco) for 21 days. Media was changed every 3rd day. At day 21, cells were fixed with 4% PFA for 15 minutes, and calcium-phosphate complexes were stained with Alizarin-Red S (ARS) for 30 minutes, followed by washing four times with double distilled water. ARS bound to calcium-phosphate complexes was extracted with 20 mM acetic acid, and the concentration of the extracted dye was calculated by measuring OD_{450}. In addition to the measurements of OD_{450} values of the extracted ARS, osteocyte markers were assayed by ICC and RT-qPCR.

Adipogenic differentiation was induced by plating 1000.000 MAFs into 6-well tissue culture-treated plates in low-glucose DMEM containing 0.5 mM 3-isobuthyl-2-methylxanthine (IBMX), 50 µM indomethacin, 0.5 µM hydrocortisone, 10 µM recombinant human insulin, 10 µM troglitazone, (all from Sigma), 20% FBS, 1% P/S and 1% GlutaMax. Medium was changed every third day until day 21 of differentiation. Lipid droplets were stained by fixing the cells in 4% PFA (15 minutes), rinsing them with 60% iso-propanol followed by 15 minutes incubation with the lipophilic dye Oil-Red O (ORO) in 2:3 ratio with double distilled water. ORO was extracted from the lipid droplets by using 60% isopropanol, and the intracellular ORO concentrations were calculated by measuring OD_{506} values of the extracted dye. Adipogenic markers were assayed by ICC and RT-qPCR.

In Vitro Hepatocyte Differentiation:

We used two methods for hepatocyte differentiation published by Mallana et al [29] and Wakao et al [30]. In the first method, we recapitulated hepatic differentiation in vitro by seeding $2x10^4$ cells/cm^2 on bovine collagen I-coated dishes (Gibco) in hepatic differentiation medium (HDM; DMEM supplemented with 10% FBS, 1X insulin-transferrin-selenium (Gibco), 10 nM dexamethasone (Sigma), 0.6 mg/mL nicotinamide (Sigma)), (Fig.4). Until the second day of differentiation, HDM was supplemented with 10 ng/mL bone-morphogenic protein-4 (BMP4 by RnD), 50 ng/mL fibroblast growth factor-4 (FGF4, by Peprotech) and 100 ng/mL activin-A (R&D). Between day 2 and day 5 cells were kept

in HDM supplemented with 100 ng/mL activin-A. From day 5 to day 10 HDM with 20 ng/mL BMP4 and 50 ng/mL FGF-4 was added, and medium was changed every other day. Between day 10 and day 15 cells were fed with HDM supplemented with 100 ng/mL hepatocyte growth factor (HGF) with medium changes every other day. From day 15 to day 20 we added HDM supplied with 20 ng/mL Oncostatin-M to the cells. At day 20 of differentiation cellular samples were processed for ICC and qRT-PCR. The hepatocarcinoma cell line Hep3B was used as positive control for the ICC experiments. Mean intensities of ICC stainings for albumin and AFP in undifferentiated, differentiated MAFS and HEP3B cells were quantified using ImageJ and normalized to the mean intensities of DAPI staining.

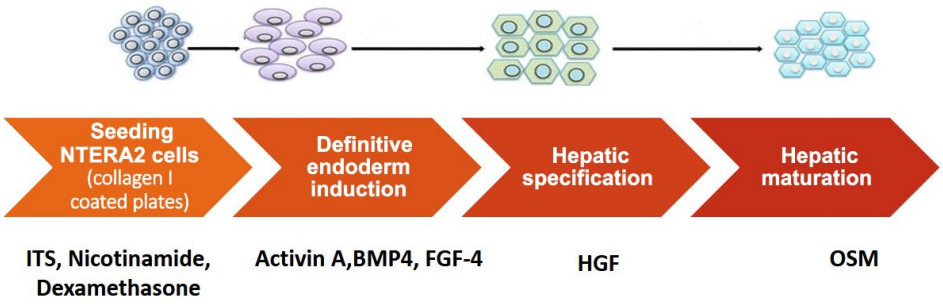

Figure 4. Optimized protocol for the in vitro differentiation of hepatocytes. *Cells were seeded into collagen-I-coated plates in hepatogenic differentiation medium (HDM) containing insulin-transferrin-selenium supplement, nicotinamide, and dexamethasone. DE-like cells were induced by activin A, BMP4 and FGF-4. Hepatic specification was promoted by the addition of HGF into the HDM, which was followed by maturation into hepatic cells with OSM. (For the exact timing of each cytokine and supplement, see the detailed description of our protocol below).*

Another method we tested for hepatic differentiation was published by Wakao et al, [30]. Briefly, cells were cultured on collagen-coated dishes with a seeding density of $2x10^4$ cells/cm^2. The hepatic differentiation medium was DMEM containing, ITS selenium supplement, 10 nM dexamethasone, 10% FBS and 100 ng/mL HGF and 50 ng/mL FGF-4.

HDM was changed every 3rd day in 14 days. Hepatic marker expression was analyzed by RT-qPCR and ICC.

3.5. Statistical Analyses:

We used GraphPad Prism (version 5) for statistical analyses. For the statistical comparison of the relative mRNA expression values of multiple markers between control and differentiated samples we used two-way ANOVA with Bonferroni post-test. The same statistical test was used to compare the expression of CD146, CD271 and SSEA3 (measured by flow-cytometry) between MAFs and DFs. Paired Student's t-test was used to compare OR and ARS concentrations between control and differentiated samples during in vitro adipocyte and osteocyte differentiation assays, respectively. Normalized mean staining intensities for ALPL, CEBPα, Nestin and albumin were compared using Kruskal-Wallis test with Dunn's post hoc test. We chose 95% confidence interval for all statistical analyses.

4. Results

Thesis 1: MAFs have a Bone-marrow Mesenchymal Stromal/Stem Cell-like Phenotype.

MAFs isolated from subcutaneous melanoma metastases displayed mesenchymal stromal cell (MSC)-like features, such as spindle shaped morphology, and high adherence to non-coated cell culture plates. To further dissect the MSC-like phenotype of MAFs, we analyzed the expression of MSC-specific cell surface molecules by flow cytometry, (Fig.5). We showed that MAFs are MSC-like cells expressing canonical MSC markers CD73, CD90, and CD105. To address whether MAFs have MSC-like mesodermal lineage differentiation, we exposed MAFs to *in vitro* osteogenic and adipogenic differentiation media, (Fig.6). MAFs accumulated calcium-phosphate deposits upon *in vitro* osteogenic differentiation (Fig.6A), and lipid droplets were enriched in MAF cultures during *in vitro* adipocyte differentiation, (Fig.6B). By conducting RT-qPCR measurements, we detected the osteocyte markers *ALPL* and *BGLAP* (Fig.6C), and adipocyte markers *PPARG* and *CEBPA* in differentiated MAFs, (Fig.6D). Furthermore, we detected the expression of osteogenic marker alkaline phosphatase (ALPL, Fig.7A, C), and adipogenic marker CCAAT enhancer binding protein α (CEBPα, Fig.7B, D) in differentiated MAFs. These results indicate, that MAFs display MSC-like cell surface marker expression, and they generate osteocytes and adipocytes *in vitro*.

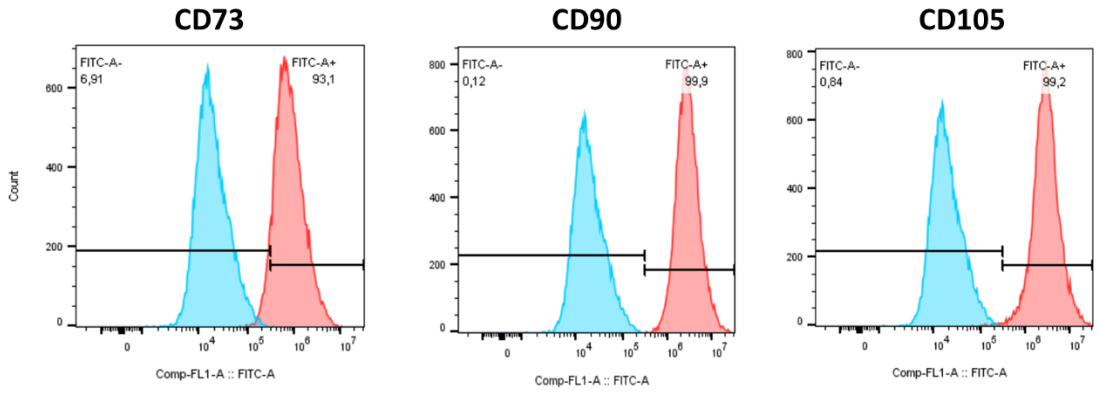

Figure 5. MAFs have a bone-marrow MSC-like phenotype. *(A) Expression of canonical MSC markers CD73, CD90 and CD105 measured by flow cytometry. 200.000-300.000 cells/ sample were labeled with FITC-conjugated anti-CD73, anti-CD90 and anti-CD105 antibodies (N=5 MAFs and DFs from different donors were measured, experiments were repeated three times).*

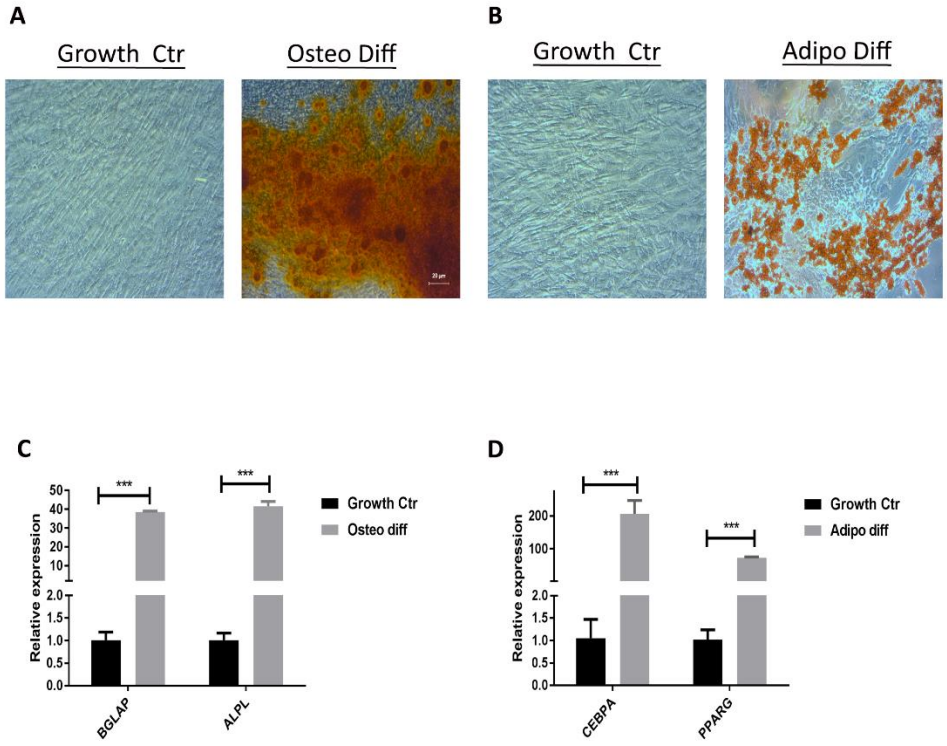

Figure 6. MAFs have a bone marrow MSC-like mesodermal differentiation potential *MAFs generate mesodermal lineage cells, osteocytes, and adipocytes. Representative images showing calcium-phosphate complexes of osteocytes stained with Alizarin Red S (A), while adipocyte-specific lipid droplets were stained with Oil Red O (B), respectively, (scalebar; 20 µM). Osteocyte and adipocyte differentiation were also characterized by RT-qPCR measurements for osteocyte markers (BGLAP, ALPL, C) and adipocyte markers (CEBPα, PPARγ, D). Relative mRNA expression values are shown compared. (GAPDH was used as housekeeping control, and undifferentiated samples were used as normalization controls. ***: $p < 0.001$). (All experiments with MAFs from N=5 different donors were repeated three times).*

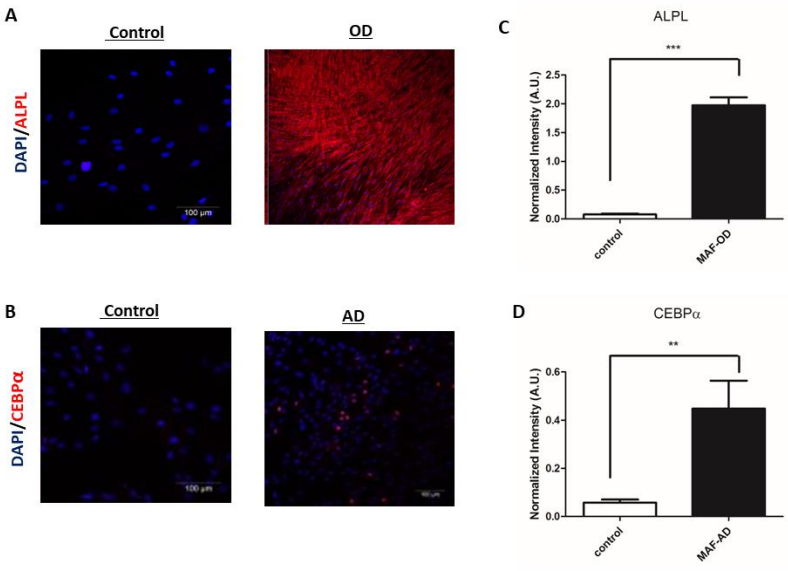

Figure 7. Expression of osteocyte marker ALPL and adipocyte marker CEBPα in MAFs upon osteogenic and adipogenic differentiation, respectively. *(A) Immunocytochemical staining of osteogenic marker alkaline phosphatase in undifferentiated MAFs and MAF-derived osteocytes. (B) Immunocytochemical staining of the adipogenic marker CEBPα in undifferentiated MAFs and MAF-derived adipocytes (B), (scalebar; 100 µm). Mean Intensities of ALPL staining in MAF derived osteocytes (C), and CEBPα in MAF-derived adipocytes normalized to DAPI. (***: P < 0.01; **: 0.01< p < 0.05) (All experiments with MAFs from N=5 different donors were repeated three times).*

Thesis 2: NTERA2 cells undergo *in vitro* neural, hepatic, and osteogenic differentiation.

We showed, that NTERA2 cells express pluripotency markers ($Oct_{3/4}$, NANOG, TRA-160, Sox2, Fig.8), [I]. By using NTERA2 cells, we optimized our methods for *in vitro* neural (Fig.9), hepatocyte (Fig.10) and osteogenic lineage differentiation, (Fig.11). By using the A172 and HEP3B immortalized cell lines as positive controls for *in vitro* characterizations, we demonstrated the generation of neural and hepatic lineage cells from NTERA2 cells. NTERA2-derived neural lineage cells expressed markers of neural stem cells, such as Nestin, MAP2 and neuronal progenitor cell marker ENO2. NTERA-derived hepatic lineage

cells displayed markers of fetal hepatocytes, including albumin, AFP and CK18. In addition, osteogenic differentiation of NTERA2 cells produced calcium-phosphate deposits in the cell cultures, and cells expressing osteogenic markers BGLAP and ALPL. Our results underpin the potential of NTERA2 clone D1 cells to serve as a cost-effective source of cellular positive control for studying pluripotent stem cell traits of induced pluripotent stem cells and adult tissue stem cells, such as MUSE cells.

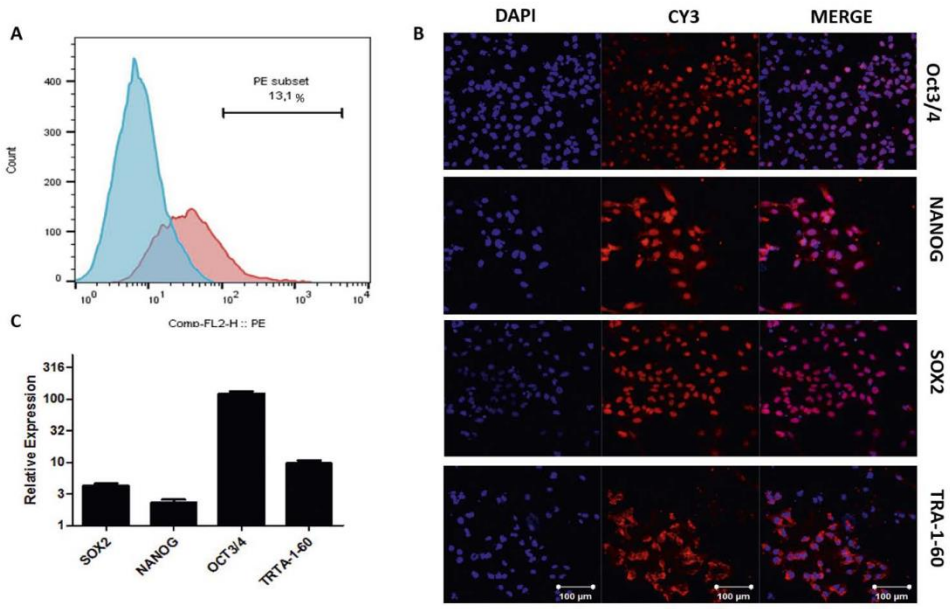

Figure 8. Pluripotent stem cell markers expression on NTERA2 clone D1 cells were analyzed by flow-cytometry, ICC, and qRT-PCR. *(A) 200.000-500.000 NTERA2 cells were stained with biotin-conjugated anti-SSEA3 antibody, which was followed by incubation with PE-conjugated streptavidin. Percentage of SSEA3+ cells (red histogram) were analyzed by flow cytometry, NTERA2 cells without primary antibody staining were used as control (blue histogram). (B) Immunocytochemical staining of NTERA2 cells with antibodies against pluripotency markers Oct3/4, NANOG, Sox2 and TRA-1-60. Nuclei were stained with DAPI, (scalebar; 100 µm). (C) Relative mRNA expression of the pluripotency markers was measured by qRT-PCR. TaqMan probe for GAPDH was used as housekeeping control, and normal dermal fibroblast samples were used as normalization control for the measurements. (Experiments were repeated three times)*

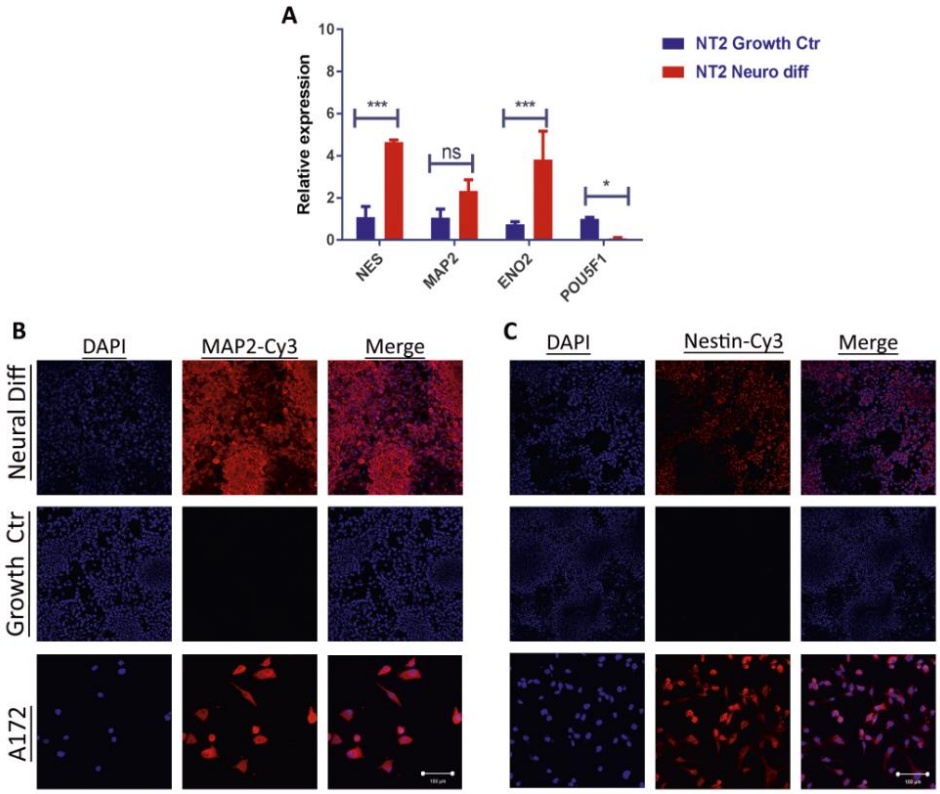

Figure 9. Neural lineage differentiation of NTERA2 cells. *Significant increase in neural lineage markers and decrease in the relative mRNA expression of pluripotency marker POU5F1 were measured by qRT-PCR. (GAPDH was used as a housekeeping control, and undifferentiated NTERA2 cells were used as normalization control for the experiments). (B) Expression of MAP2 and Nestin (C) were detected in differentiated and positive control (A172) cells, but not in undifferentiated NTERA2 cells, (scalebar; 100µm). (*: $p < 0.05$, ***: $p < 0.001$, ns: non-significant. Three repeated experiments were made.).*

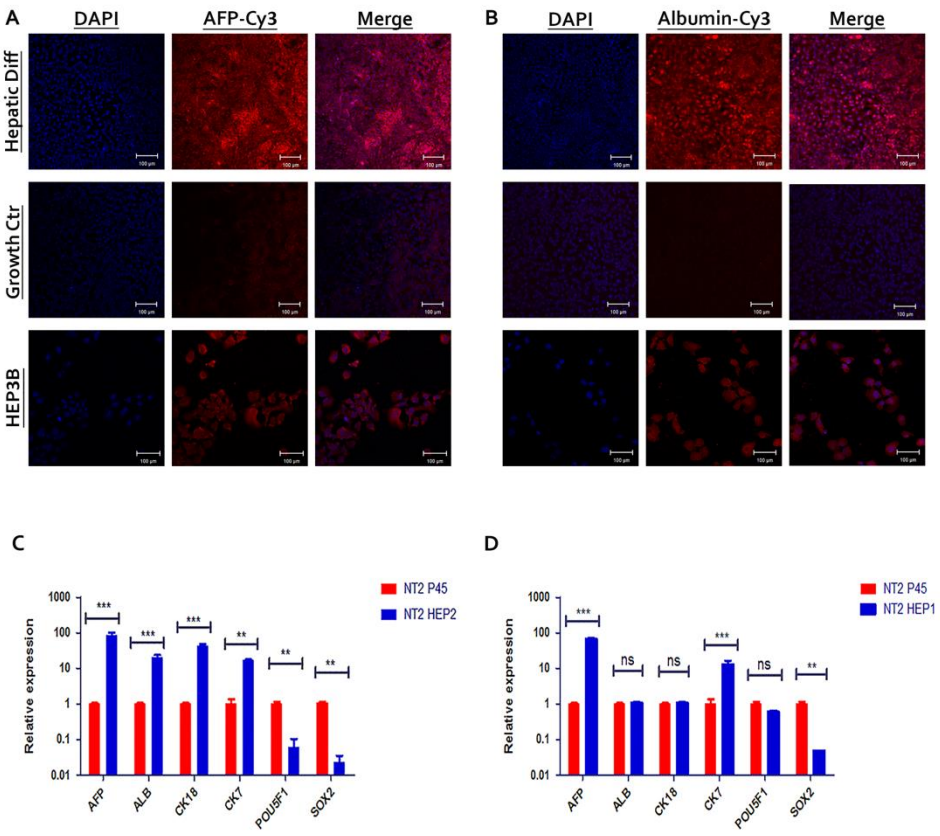

Figure 10. In vitro differentiation of NTERA2 cells towards hepatic lineages. *(A) Expression of AFP and albumin (B) were detected in NTERA2 cells differentiated by HEP2 method, and positive control (HEP3B) cells, but not in undifferentiated NTERA2 cells, (scalebar; 100µm). (C) Significant increase in hepatic lineage markers (AFP, ALB, CK18, CK7) and significant decrease in the relative mRNA expression of pluripotency markers POU5F1 and SOX2 were measured by qRT-PCR. (D) In contrast, no significant difference in the expression of ALB, CK18 and POU5F1 were detected when we utilized the HEP1 method. (***: $p < 0.01$, **: $0.01 < p < 0.05$. Experiments were repeated three times).*

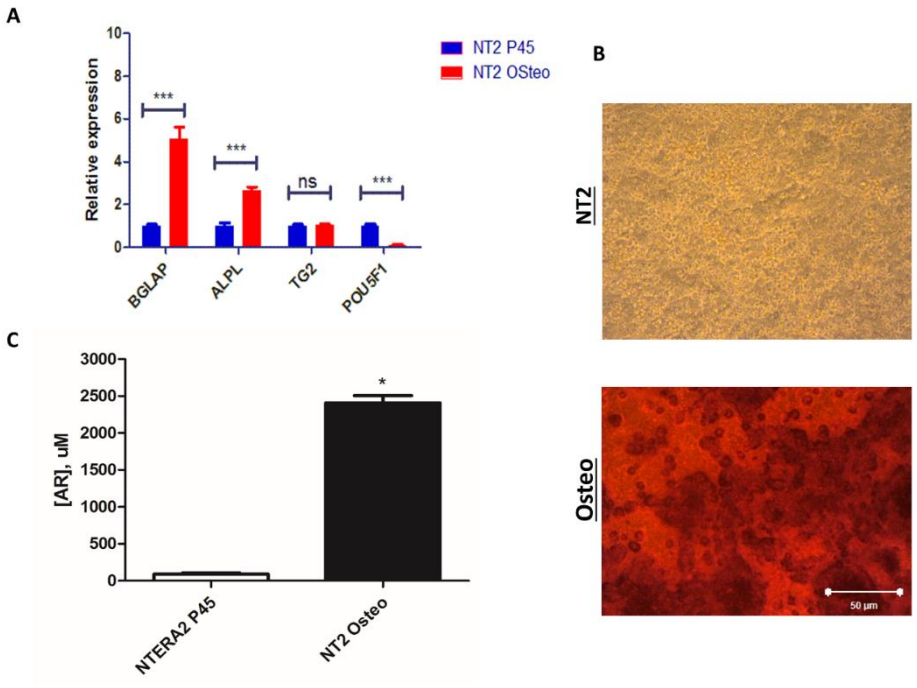

Figure 11. Osteocyte lineage differentiation of NTERA2 cells. *(A) Significant increase in osteocyte lineage markers (BGLAP2, ALPL, TG3), and decrease in the relative mRNA expression of pluripotency marker POU5F1 were measured by qRT-PCR. (B) ARS staining revealed an increased number of calcium-phosphate deposits in differentiated NTERA2 cells, but not in undifferentiated NTERA2 cells, (scalebar; 50µm). (C) Quantitation of the extracted ARS by OD_{450} measurements in undifferentiated cells and NTERA2-derived osteocytes. (*: $p < 0.05$, ***: $p < 0.001$, ns: non-significant. Three repeated experiments were made.)*

Thesis 3: MAFs Have Enhanced Tri-lineage Differentiation Potential Compared to Normal Dermal Fibroblasts.

We compared mesodermal lineage differentiation potential of MAFs to normal dermal fibroblasts by using our *in vitro* osteogenic and adipogenic differentiation assays. MAFs generated significantly higher number of mesodermal lineage cells, than normal dermal fibroblasts, (Fig.12, Fig.13). Next, we analyzed multilineage differentiation of MAFs in our *in vitro* ectodermal (neural) and endodermal (hepatic) lineage differentiation assays, which were optimized on pluripotent NTERA2 cells, (Fig.14). In addition to their enhanced mesodermal lineage generation potential, melanoma associated fibroblasts generated MAP+Nestin+ ectodermal (Fig.14B, D, F), and AFP+albumin+ endodermal lineage cells (Fig.14A, C, E).

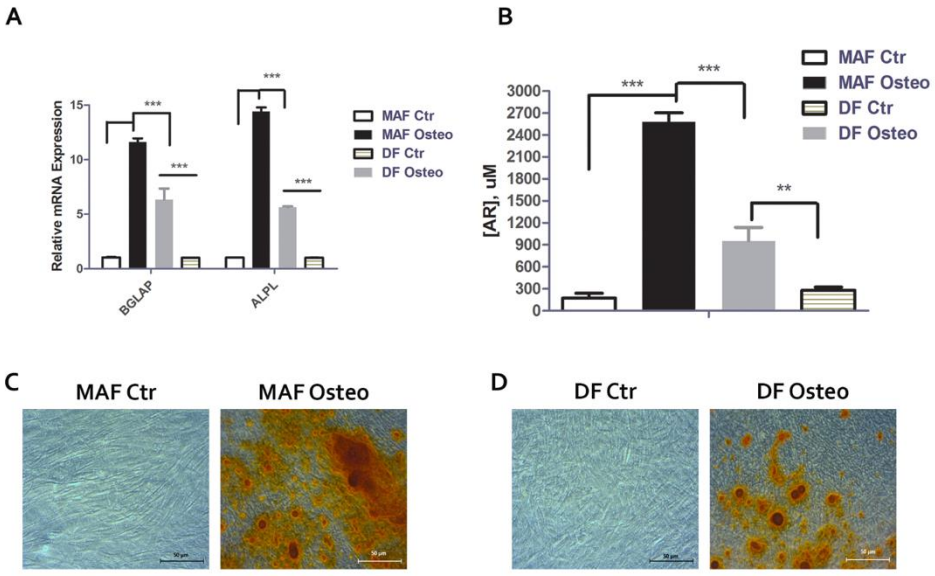

Figure 12. MAFs have significantly higher osteogenic differentiation potential than DFs. *(A) Relative mRNA expression of osteogenic markers BGLAP and ALPL in control and differentiated MAFs and DFs, measured by qRT-PCR. GAPDH was used as housekeeping control, expression values were normalized to control/undifferentiated samples. (B) Concentration of ARS dye extracted from calcium phosphate complexes of control and differentiated MAFs and DFs, (given in µM). Representative images showing ARS staining of calcium-phosphate complexes of DF- (C) and MAF-derived osteocytes (D) compared to their undifferentiated controls, (scalebar; 50 µm). (***: $p < 0.01$, **: $0.01 < p < 0.05$. N= 5 MAFs and DFs from different donors were used for the experiments, experiments were repeated three-times).*

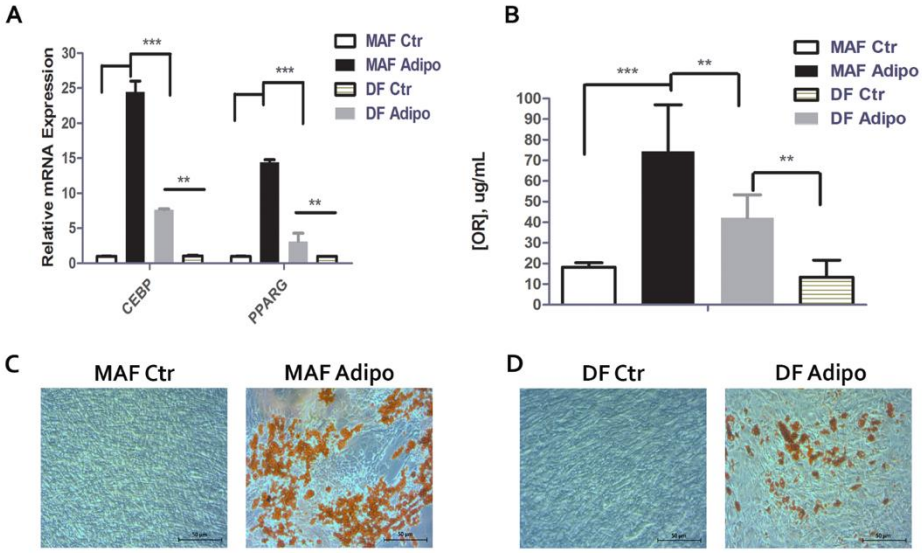

Figure 13. MAFs have significantly higher adipogenic differentiation potential than DFs. *(A) Relative mRNA expression of adipogenic markers PPARG and CEBPα in control and differentiated MAFs and DFs, measured by qRT-PCR. GAPDH was used as housekeeping control, expression values were normalized to control/undifferentiated samples. (B) Concentration of ORO dye extracted from lipid droplets of control and differentiated MAFs and DFs, (given in µg/mL). Representative images showing ORO staining of lipid droplets in DF- (C) and MAF-derived adipocytes (D) compared to their undifferentiated controls, (scalebar; 50 µm). (***: $p < 0.01$, **: $0.01 < p < 0.05$. N= 5 MAFs and DFs from different donors were used for the experiments, experiments were repeated three-times).*

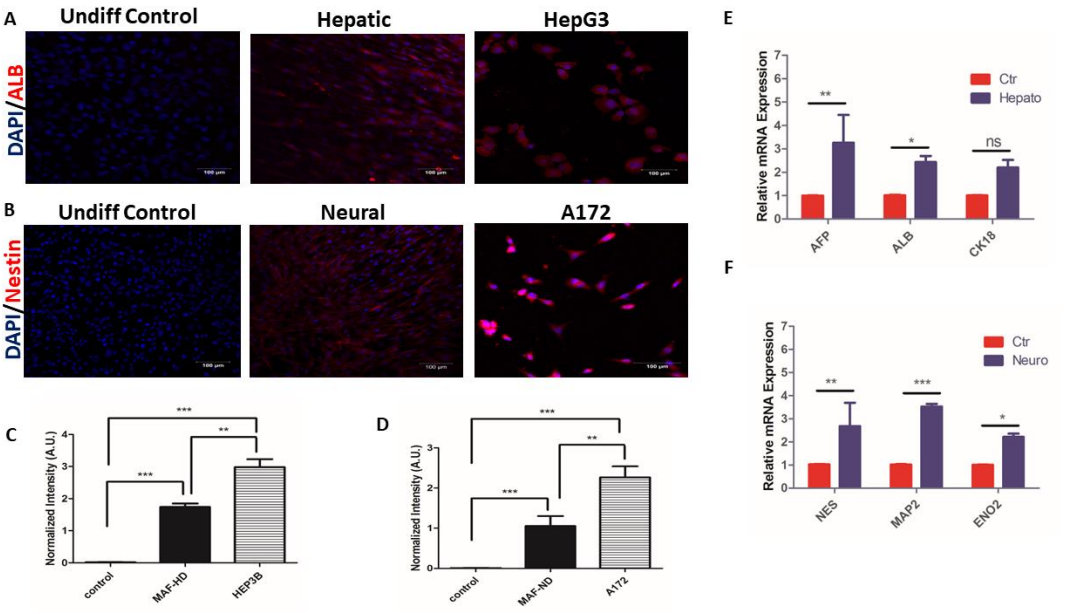

Figure 14. In vitro neural and hepatic differentiation of MAFs. *(A) MAFs were differentiated towards neural lineage cells and characterized for the expression of Nestin by ICC. Nuclei were stained with DAPI. Left: undifferentiated control MAFs, middle: differentiated MAFs, right: A172 cells (positive control), (scalebar; 100 um). (B) MAFs were differentiated towards hepatic lineage cells and characterized for the expression of albumin (ALB) by ICC. Nuclei were stained with DAPI. Left: undifferentiated control MAFs, middle: differentiated MAFs, right: HEP3B cells (positive control), (scalebar; 100 µM). (C) Quantitation of the mean staining intensities for ALB in undifferentiated controls, hepatic differentiation of MAFs and HEP3B cells, normalized for mean staining intensity of DAPI (arbitrary units). (***: $p < 0.01$, **: $0.01 < p < 0.05$). (D) Quantitation of the mean staining intensities for Nestin in undifferentiated controls, neural differentiation of MAFs and A172 cells, normalized for mean staining intensity of DAPI (arbitrary units). (***: $p < 0.01$, **: $0.01 < p < 0.05$). (E) Neural markers Nestin, MAP2 and ENO2 were upregulated, as shown by qRT-PCR. (GAPDH was used as housekeeping control, samples were normalized to undifferentiated controls.) (F) Hepatic markers AFP, ALB and CK18 were upregulated, as shown by qRT-PCR. (GAPDH was used as housekeeping control, samples were normalized to undifferentiated controls). (***: $p < 0.01$, **: $0.01 < p < 0.05$, *: $p \leq 0.05$, ns: non-significant. N=3 MAFS from different donors were used, experiments were repeated two times.)*

<u>Thesis 3: MAFs harbor MUSE cells, CD146+ and CD271+ stem cell subsets</u>.

By utilizing flow-cytometric measurements, we showed that MAFs contain stromal stem cell subsets, such as CD271+, CD146+ and SSEA3+ cells, (Fig.15). SSEA3+ cells were described as multi-lineage differentiating, stress enduring cells, which express pluripotent stem cell markers, modulate inflammatory immune responses, and give rise to melanocytes [6], [26]. To further characterize the SSEA3+ cell subset in melanomas, we isolated SSEA3+CD90+ stromal cells from MAFs by fluorescence-activated cell sorting (Fig.16A) and analyzed the expression of pluripotency markers in these cells.

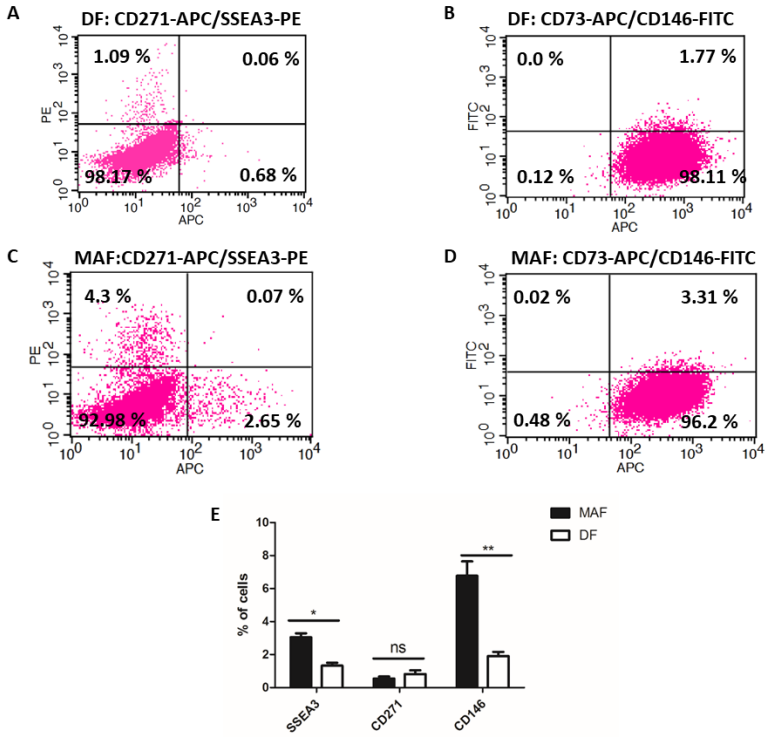

Figure 15. Stem-cell markers expression in normal dermal fibroblasts and MAFs. *Flow-cytometry dot plots made from measurements of DFs (A-B) and MAFs (C-D) double stained with SSEA3-PE/CD271-APC (A, C) and CD73-APC/CD146-FITC (B, D) antibodies. (E): Percentages of MAFs and DFs expressing SSEA3, CD271 and CD146. MAFs have significantly higher number of SSEA3+ and CD146+ cells. (**; 0.01< p < 0.05, *; p < 0.05, ns: non-significant. N=5 DF and MAF samples from different donors were measured, 20.000 events/sample were recorded. Experiments were repeated three times.).*

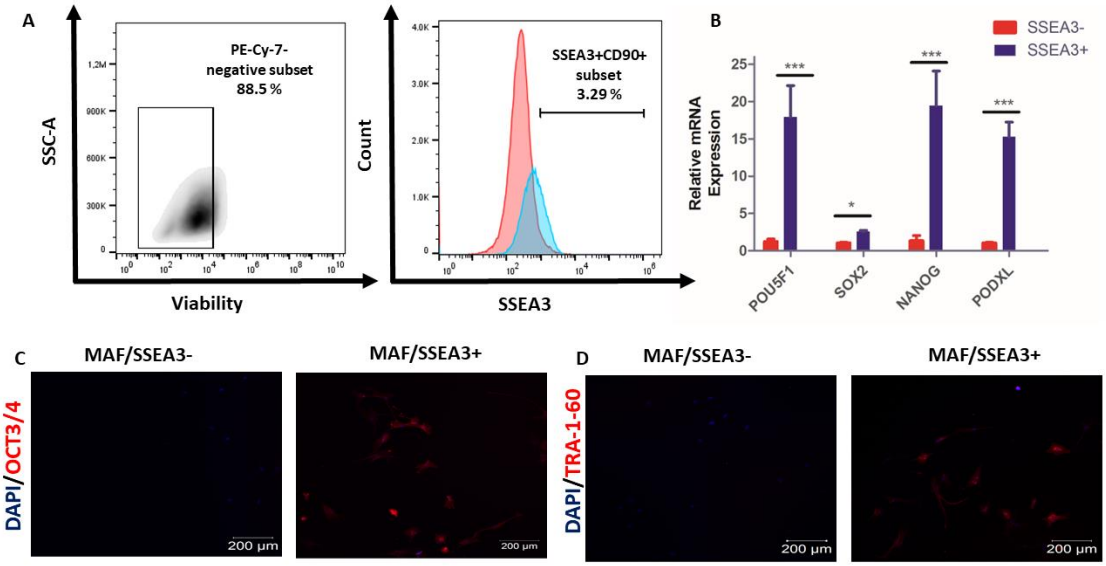

Figure 16. MAFs encompass MUSE cells. *(A) Isolation of MUSE cells by* FACS. *Cytometry gates were set to viable cells (lacking PE-Cy-7 staining), and then for SSEA3+ population. (5-10 million cells from N=3 MAFs from different donors were used. Red histogram represents unstained control, and the blue histogram shows SSEA+ cells before FACS). (B) Relative mRNA expression of pluripotent stem cell markers POU5F1, SOX2, NANOG and PODXL were analyzed by qRT-PCR. (GAPDH was used as housekeeping control, expression values were normalized to SSEA3- sorted samples). (C) Sorted SSEA3+ cells, but not SSEA3-negative cells express $Oct_{3/4}$ and TRA-1-60, as demonstrated by ICC. (scalebar; 200 µm, nuclei were stained with DAPI). (***: $p < 0.01$, *: $p \leq 0.05$, N= 5 MAFs from different donors were used, experiments were repeated two-times).*

We showed by ICC stainings (Fig.16C-D) and qRT-PCR measurements (Fig.16B) that SSEA3+ MAF cells express pluripotent stem cell marker $Oct_{3/4}$, SOX2, NANOG and TRA-1-60. In conclusion, MAFs encompass SSEA3+ MUSE cells, which express not only the canonical stromal markers (CD90, CD105), but also pluripotent stem cell markers ($Oct_{3/4}$, Sox2, NANOG, TRA-1-60).

Thesis 5: MUSE cells from MAFs Generate Melanocyte Lineage Cells.

After the identification of MUSE cells in MAFs, we examined their ability to generate melanocyte lineage cells *in vitro*, (Fig.17). MUSE cells from MAFs, but not SSEA3- non-MUSE cells differentiate into melanocyte lineage cells in vitro, which have elongated, dendritic morphology and express Melan-A. Furthermore, additional melanocyte lineage markers, such as MITF, DCT and TYRP1 were also upregulated in SSEA3+ cells, but not in SSEA3- (non-MUSE) cells upon *in vitro* melanocytic differentiation.

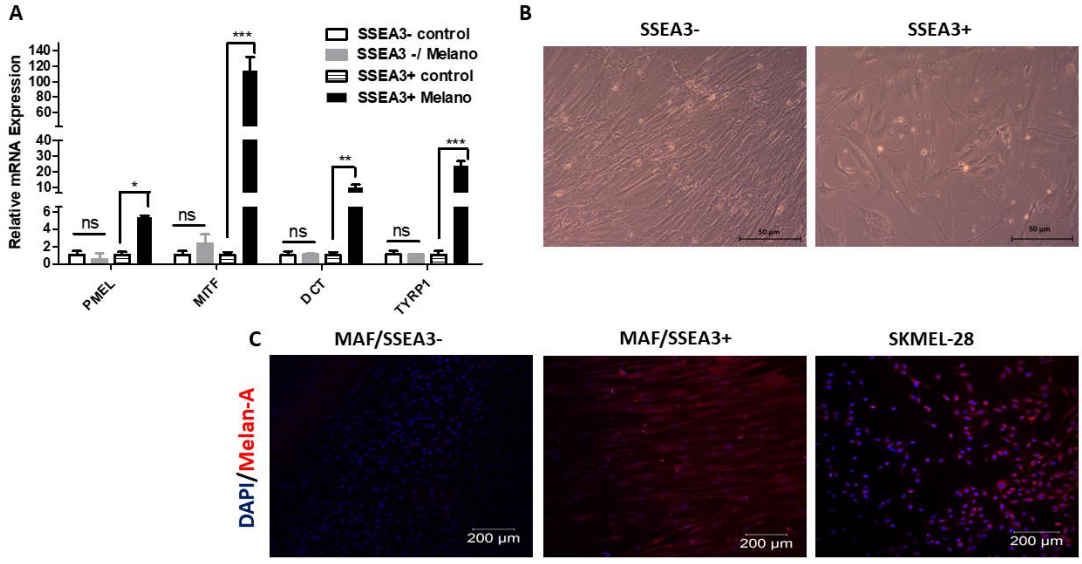

Figure 17. MAF-MUSE cells give rise to melanocyte lineage cells in vitro. *MUSE cells from MAFs were separated as viable CD90+SSEA3+ cells from viable CD90+SSEA3- cells by FACS-sorting. Sorted SSEA3+ and SSEA3- cells were seeded into fibronectin-coated plates, and melanocyte lineage cells were induced within 6 weeks. (A) Upregulation of melanocyte markers PMEL, MITF, DCT and TYRP1 were observed in sorted SSEA+ MAFs by qRT-PCR. GAPDH was used as housekeeping control, and relative mRNA expressions values were normalized to undifferentiated control samples. (***: p< 0.01, **; 0.01< p < 0.05, *; p < 0.05). (B) SSEA3+, but not SSEA3- cells acquired elongated, dendritic morphology. (Light microscopic images at day 42 of differentiation, scalebar; 50 µm). (C) Expression of Melan-A was confirmed in SSEA3+ cells (up/ middle), but not in SSEA3- cells (down/middle) by ICC, compared to undifferentiated control (left panel) and positive control (SKMEL-28 cells, right side image). (Nuclei were stained with DAPI, scalebar; 200 µm). (N= 5 MAFs from different donors were used for the experiments).*

5. Potential Application of the Results

CAFs are the most abundant cells of the tumor-microenvironment, and through intricate interactions with the tumor-microenvironment they play central roles in orchestrating cancer growth, immunosuppression, metastasis, and drug resistance. Although molecular targeting strategies abrogating CAF functions have emerged [31], specific markers enabling the identification of CAFs are still missing. In contrast to the cancer cells, CAFs have a lower proliferation rate, therefore they are less targetable by conventional chemotherapeutic approaches. On the other hand, the identification of CAF-specific molecular markers would enhance the selective elimination of tumor-promoting CAF subsets. Given the high heterogeneity of CAFs, elucidating the stem cell sources of CAFs is a key step in the effective targeting and abrogation of the stromal supply of cancers.

Malignant melanoma is an extremely aggressive and drug-resistant cancer associated with high mortality and poor prognosis. In concert with similar studies our lab reported the immunosuppressive action of MAFs, [32], [II], yet limited information is available on the phenotypic composition, stem cell sources and differentiation plasticity of MAFs. Here, I demonstrated that melanoma associated fibroblasts have an MSC-like molecular phenotype (Fig.5-7), and enhanced capacity for in vitro multilineage differentiation. The advanced differentiation potential of MAFs raises the possibility of targeting these cells by chemical agents promoting their differentiation to other cell types, (for e.g., adipocytes) with subsequent loss of their pro-tumorigenic functions [33].

To analyze the ectodermal (neural, melanocyte), mesodermal (osteocyte, adipocyte) and endodermal (hepatocyte) lineage differentiation of MAFS, we optimized the *in vitro* tri-lineage differentiation assays by using the NTERA2 clone D1 cel line. We showed, that NTERA2 cells express pluripotent stem cell markers, and they generate neural, hepatocyte and osteocyte lineage cells, (Fig.9-11). Therefore, our results support NTERA2 cells as a model system, which is suitable for analyzing tri-lineage differentiation of pluripotent cell lines and subtypes, such as MUSE cells.

In addition to their MSC-like phenotype, we identified stem cell subsets in MAFs, which might be sources of the tumor stroma due to their self-renewal and differentiation potential. We showed, that MAFs harbor the CD146+ and CD271+ stem cell subsets,

(Fig.15), which are implicated in immunomodulation and angiogenesis in homeostatic tissues, [34], [35]. It remains to be seen how the targeting of these cell subsets affects immunosuppression and angiogenesis in melanoma. In addition to the CD146+ and CD271+ cells, we also demonstrated the presence of multi-lineage differentiating, stress enduring cells in MAFs, (Fig.16), a multipotent stem cell subpopulation awakened by cellular stress, inflammatory and tissue damage signals. Given their ability to suppress inflammatory T-cell responses [8], the significance of MUSE cells in tumor growth and resistance remains an intriguing question, which warrants further studies. Furthermore, the implications of enhanced melanocytic differentiation of MUSE cells from MAFs (Fig.17) needs further investigation in the context of melanoma growth.

Taken together, our results showed that specific stromal cell subsets reside in human malignant melanomas with stem cell properties. We identified three stromal stem cell subsets among MAFs: CD146+ cells, CD271+ cells and MUSE cells. These stem cell subsets might contribute to the enhanced capacity of MAFs for the generation of mesodermal lineage cells and multilineage differentiation. Contribution of these MAF subpopulations to the growth and spreading of melanomas requires further studies, as well as their suitability as cellular targets for novel anti-cancer therapies.

6. Acknowledgements

I am deeply thankful to Professor Dr. Sarolta Kárpáti to allow me to participate the Stem Cell Research Group. I would like to express my gratitude to my supervisors, Dr. Krisztián Németh and Dr. Miklós Gyöngy for their contribution to study design, supervision, and manuscripts preparation. I am grateful to Dr. Balázs Mayer, Dr. Zoltán Pos, Dr. Barbara Molnár-Érsek and Dr. Gábor Barna for their great amount of help in learning flow cytometry, cell sorting techniques, statistical analysis, and data interpretation. I would like to thank dr. Pálma Silló, Mercédesz Mazán, Adrien Suba for providing me training and methodological insight into fibroblast isolation and real-time quantitative PCR measurements. I am also thankful to my former and current colleagues, Szilvia Barsi, Anna Hajdara and Dr. Cakir Ugur for their helpful, cooperative, and friendly attitude and all support in my scientific work.

7. References:

[1]: Feldman, A., Mukha, D., Maor, I. I., Sedov, E., Koren, E., Yosefzon, Y., Shlomi, T., & Fuchs, Y. (2019). Blimp1^{+} cells generate functional mouse sebaceous gland organoids in vitro. *Nature communications*, *10*(1), 2348.

[2]: Heitman, N., Sennett, R., Mok, K. W., Saxena, N., Srivastava, D., Martino, P., Grisanti, L., Wang, Z., Ma'ayan, A., Rompolas, P., & Rendl, M. (2020). Dermal sheath contraction powers stem cell niche relocation during hair cycle regression. *Science (New York, N.Y.)*, *367*(6474), 161–166.

[3]: Lim, X., Tan, S. H., Yu, K. L., Lim, S. B., & Nusse, R. (2016). Axin2 marks quiescent hair follicle bulge stem cells that are maintained by autocrine Wnt/β-catenin signaling. *Proceedings of the National Academy of Sciences of the United States of America*, *113*(11), E1498–E1505.

[4]: Hsu, Y. C., Li, L., & Fuchs, E. (2014). Emerging interactions between skin stem cells and their niches. *Nature medicine*, *20*(8), 847–856.

[5]: Vaculik, C., Schuster, C., Bauer, W., Iram, N., Pfisterer, K., Kramer, G., Reinisch, A., Strunk, D., & Elbe-Bürger, A. (2012). Human dermis harbors distinct mesenchymal stromal cell subsets. *The Journal of investigative dermatology*, *132*(3 Pt 1), 563–574.

[6]: Heneidi, S., Simerman, A. A., Keller, E., Singh, P., Li, X., Dumesic, D. A., & Chazenbalk, G. (2013). Awakened by cellular stress: isolation and characterization of a novel population of pluripotent stem cells derived from human adipose tissue. *PloS one*, *8*(6), e64752.

[7]: Bernardo, M. E., & Fibbe, W. E. (2013). Mesenchymal stromal cells: sensors and switchers of inflammation. *Cell stem cell*, *13*(4), 392–402.

[8]: Gimeno, M. L., Fuertes, F., Barcala Tabarrozzi, A. E., Attorressi, A. I., Cucchiani, R., Corrales, L., Oliveira, T. C., Sogayar, M. C., Labriola, L., Dewey, R. A., & Perone, M. J. (2017). Pluripotent Nontumorigenic Adipose Tissue-Derived Muse Cells have Immunomodulatory Capacity Mediated by Transforming Growth Factor-β1. *Stem cells translational medicine*, *6*(1), 161–173.

[9]: Mao, X., Xu, J., Wang, W., Liang, C., Hua, J., Liu, J., Zhang, B., Meng, Q., Yu, X., & Shi, S. (2021). Crosstalk between cancer-associated fibroblasts and immune cells in the tumor microenvironment: new findings and future perspectives. *Molecular cancer*, *20*(1), 131.

[10]: Arpinati, L., & Scherz-Shouval, R. (2023). From gatekeepers to providers: regulation of immune functions by cancer-associated fibroblasts. *Trends in cancer*, *9*(5), 421–443.

[11]: Qiao, Y., Zhang, C., Li, A., Wang, D., Luo, Z., Ping, Y., Zhou, B., Liu, S., Li, H., Yue, D., Zhang, Z., Chen, X., Shen, Z., Lian, J., Li, Y., Wang, S., Li, F., Huang, L., Wang, L., Zhang, B., Zhang, Y. (2018). IL6 derived from cancer-associated fibroblasts promotes chemoresistance via CXCR7 in esophageal squamous cell carcinoma. *Oncogene*, *37*(7), 873–883.

[12]: Huang, W. Y., Lin, Y. S., Lin, Y. C., Nieh, S., Chang, Y. M., Lee, T. Y., Chen, S. F., & Yang, K. D. (2022). Cancer-Associated Fibroblasts Promote Tumor Aggressiveness in Head and Neck Cancer through Chemokine Ligand 11 and C-C Motif Chemokine Receptor 3 Signaling Circuit. *Cancers*, *14*(13), 3141.

[13]: Miki, Y., Yashiro, M., Okuno, T., Kitayama, K., Masuda, G., Hirakawa, K., & Ohira, M. (2018). CD9-positive exosomes from cancer-associated fibroblasts stimulate the migration ability of scirrhous-type gastric cancer cells. *British journal of cancer*, *118*(6), 867–877.

[14]: Kay, E. J., Paterson, K., Riera-Domingo, C., Sumpton, D., Däbritz, J. H. M., Tardito, S., Boldrini, C., Hernandez-Fernaud, J. R., Athineos, D., Dhayade, S., Stepanova, E., Gjerga, E., Neilson, L. J., Lilla, S., Hedley, A., Koulouras, G., McGregor, G., Jamieson, C., Johnson, R. M., Park, M., … Zanivan, S. (2022). Cancer-associated fibroblasts require proline synthesis by PYCR1 for the deposition of pro-tumorigenic extracellular matrix. *Nature metabolism*, *4*(6), 693–710.

[15]: Lv, C., Dai, H., Sun, M., Zhao, H., Wu, K., Zhu, J., Wang, Y., Cao, X., Xia, Z., & Xue, C. (2017). Mesenchymal stem cells induce epithelial mesenchymal transition in melanoma by paracrine secretion of transforming growth factor-β. *Melanoma research*, *27*(2), 74–84.

[16]: Manoukian, P., Bijlsma, M., & van Laarhoven, H. (2021). The Cellular Origins of Cancer-Associated Fibroblasts and Their Opposing Contributions to Pancreatic Cancer Growth. *Frontiers in cell and developmental biology*, *9*, 743907.

[17]: Hutchins, D., & Steel, C. M. (1994). Regulation of ICAM-1 (CD54) expression in human breast cancer cell lines by interleukin 6 and fibroblast-derived factors. *International journal of cancer*, *58*(1), 80–84.

[18]: Miki, Y., Yashiro, M., Okuno, T., Kitayama, K., Masuda, G., Hirakawa, K., & Ohira, M. (2018). CD9-positive exosomes from cancer-associated fibroblasts stimulate the migration ability of scirrhous-type gastric cancer cells. *British journal of cancer*, *118*(6), 867–877.

[19]: Pan, J., Ma, Z., Liu, B., Qian, H., Shao, X., Liu, J., Wang, Q., & Xue, W. (2023). Identification of cancer-associated fibroblasts subtypes in prostate cancer. *Frontiers in immunology*, *14*, 1133160.

[20]: Gu, L., Liao, P., & Liu, H. (2022). Cancer-associated fibroblasts in acute leukemia. *Frontiers in oncology*, *12*, 1022979.

[21]: Jamal, S. M. E., Alamodi, A., Wahl, R. U., Grada, Z., Shareef, M. A., Hassan, S. Y., Murad, F., Hassan, S. L., Santourlidis, S., Gomez, C. R., Haikel, Y., Megahed, M., & Hassan, M. (2020). Melanoma stem cell maintenance and chemo-resistance are mediated by CD133 signal to PI3K-dependent pathways. *Oncogene*, *39*(32), 5468–5478.

[22]: Tejera-Vaquerizo, A., Nagore, E., Meléndez, J. J., López-Navarro, N., Martorell-Calatayud, A., Herrera-Acosta, E., Traves, V., Guillén, C., & Herrera-Ceballos, E. (2012). Chronology of metastasis in cutaneous melanoma: growth rate model. *The Journal of investigative dermatology*, *132*(4), 1215–1221.

[23]: Hodis, E., Watson, I. R., Kryukov, G. V., Arold, S. T., Imielinski, M., Theurillat, J. P., Nickerson, E., Auclair, D., Li, L., Place, C., Dicara, D., Ramos, A. H., Lawrence, M. S., Cibulskis, K., Sivachenko, A., Voet, D., Saksena, G., Stransky, N., Onofrio, R. C., Winckler, W., … Chin, L. (2012). A landscape of driver mutations in melanoma. *Cell*, *150*(2), 251–263.

[24]: Plaks, V., Kong, N., & Werb, Z. (2015). The cancer stem cell niche: how essential is the niche in regulating stemness of tumor cells? *Cell stem cell*, *16*(3), 225–238.

[25]: Yamauchi, T., Kuroda, Y., Morita, T., Shichinohe, H., Houkin, K., Dezawa, M., & Kuroda, S. (2015). Therapeutic effects of human multilineage-differentiating stress enduring (MUSE) cell transplantation into infarct brain of mice. *PloS one*, *10*(3), e0116009.

[26]: Tsuchiyama, K., Wakao, S., Kuroda, Y., Ogura, F., Nojima, M., Sawaya, N., Yamasaki, K., Aiba, S., & Dezawa, M. (2013). Functional melanocytes are readily reprogrammable from multilineage-differentiating stress-enduring (muse) cells, distinct stem cells in human fibroblasts. *The Journal of investigative dermatology*, *133*(10), 2425–2435.

[27]: Gimeno, M. L., Fuertes, F., Barcala Tabarrozzi, A. E., Attorressi, A. I., Cucchiani, R., Corrales, L., Oliveira, T. C., Sogayar, M. C., Labriola, L., Dewey, R. A., & Perone, M. J. (2017). Pluripotent Nontumorigenic Adipose Tissue-Derived Muse Cells have Immunomodulatory Capacity Mediated by Transforming Growth Factor-β1. *Stem cells translational medicine*, *6*(1), 161–173.

[28]: Yamauchi, T., Yamasaki, K., Tsuchiyama, K., Koike, S., & Aiba, S. (2017). A quantitative analysis of multilineage-differentiating stress-enduring (Muse) cells in human adipose tissue and efficacy of melanocytes induction. *Journal of dermatological science*, *86*(3), 198–205

[29]: Mallana, S. K., & Duncan, S. A. (2013). Differentiation of hepatocytes from pluripotent stem cells. *Current protocols in stem cell biology*, *26*, 1G.4.1–1G.4.13.

[30]: Wakao, S., Kitada, M., Kuroda, Y., Shigemoto, T., Matsuse, D., Akashi, H., Tanimura, Y., Tsuchiyama, K., Kikuchi, T., Goda, M., Nakahata, T., Fujiyoshi, Y., & Dezawa, M. (2011). Multilineage-differentiating stress-enduring (Muse) cells are a primary source of induced pluripotent stem cells in human fibroblasts. *Proceedings of the National Academy of Sciences of the United States of America*, *108*(24), 9875–9880.

[31]: Li L, Fukunaga-Kalabis M, Yu H, Xu X, Kong J, Lee JT, Herlyn M. Human dermal stem cells differentiate into functional epidermal melanocytes. J Cell Sci. 2010 Mar 15;123(Pt 6):853-60.

[32]: Zhou, Q., Jin, X., Zhao, Y., Wang, Y., Tao, M., Cao, Y., & Yin, X. (2024). Melanoma-associated fibroblasts in tumor-promotion flammation and antitumor immunity: novel mechanisms and potential immunotherapeutic strategies. *Human molecular genetics*, *33*(13), 1186–1193.

[33]: Beug H. (2009). Breast cancer stem cells: eradication by differentiation therapy? *Cell*, *138*(4), 623–625.

[34]: Leñero, C., Kaplan, L. D., Best, T. M., & Kouroupis, D. (2022). CD146+ Endometrial-Derived Mesenchymal Stem/Stromal Cell Subpopulation Possesses Exosomal Secretomes with Strong Immunomodulatory miRNA Attributes. *Cells*, *11*(24), 4002.

[35]: Smith, R. J. P., Faroni, A., Barrow, J. R., Soul, J., & Reid, A. J. (2021). The angiogenic potential of CD271+ human adipose tissue-derived mesenchymal stem cells. *Stem cell research & therapy*, *12*(1), 160.

8. Bibliography

List of Publications underlying the thesis:

First-authorship

[I]: Szeky, B., Mayer, B., Gyongy, M., Hajdara, A., Barsi, S., Karpati, S., & Nemeth, K. (2021). Tri-Lineage Differentiation of NTERA2 Clone D1 Cells towards Neural, Hepatic and Osteogenic Lineages in Vitro. *FOLIA BIOLOGICA*, *67*(5–6), 174–182.

Co-first authorship:

[II]: Çakır, U., Hajdara, A., Széky, B., Mayer, B., Kárpáti, S., Mezey, É., … Németh, K. (2021). Mesenchymal-Stromal Cell-like Melanoma-Associated Fibroblasts Increase IL-10 Production by Macrophages in a Cyclooxygenase/Indoleamine 2,3-Dioxygenase-Dependent Manner. *CANCERS*, *13*(24).

List of publications related to the subject of the thesis:

Hajdara, A., Çakır, U., Érsek, B., Silló, P., Széky, B., Barna, G., … Mayer, B. (2023). Targeting Melanoma-Associated Fibroblasts (MAFs) with Activated γδ (Vδ2) T Cells: An In Vitro Cytotoxicity Model. *INTERNATIONAL JOURNAL OF MOLECULAR SCIENCES*, *24*(16), 12893.

Other publications

Széky, B. (2018). The Role of Extracellular Matrix Remodeling Enzymes in Dermal Stem Cell Function. *PHD PROCEEDINGS ANNUAL ISSUES OF THE DOCTORAL SCHOOL FACULTY OF INFORMATION TECHNOLOGY AND BIONICS*, *13*, 71.

Széky, B. (2017). Investigating Molecular Markers and Regulators of Dermal Stem Cell Function. *PHD PROCEEDINGS ANNUAL ISSUES OF THE DOCTORAL SCHOOL FACULTY OF INFORMATION TECHNOLOGY AND BIONICS*, *12*, 34–34.

Balázs, S. (2016). Examination of dermal stem cells in healthy and diseased skin. *PHD PROCEEDINGS ANNUAL ISSUES OF THE DOCTORAL SCHOOL FACULTY OF INFORMATION TECHNOLOGY AND BIONICS*, *11*, 97–100.

Szeky, B., Sillo, P., Fabian, M., Mayer, B., Karpati, S., & Nemeth, K. (2016). Tumorőssejtek szerepe a melanoma progressziójában és heterogenitásában. *ORVOSI HETILAP*, *157*(34), 1339–1348.